R NUCLEAR RESEARCH

CERN /SPSLC 92-16
SPSLC / P 268

March 13, 1992

PROPOSAL FOR A STRANGELET AND PARTICLE SEARCH IN PB-PB COLLISIONS

NEWMASS Collaboration

K. Borer, F. Dittus, D. Frei, R. Klingenberg, E. Hugentobler, U. Moser, K. Pretzl*, J. Schacher, F. Stoffel, W. Volken
Berne University, Switzerland

K. Elsener, K.D. Lohmann
CERN, Geneva, Switzerland

C. Baglin, A. Bussière, J.P. Guillaud
LAPP, CNRS-IN2P3, Annecy-le-Vieux, France

J. Tuominiemi
Helsinki University, Finland

G. Appelquist, C. Bohm, B. Hovander, S. Nilsson, B. Selldèn, Q. Zhang
Stockholm University, Sweden

*Spokesperson

1. Introduction

We propose to search for long-lived massive strange matter particles, the so-called "strangelets", in Pb-Pb collisions at CERN. In this experiment, we intend to look for positively and negatively charged massive objects at 0° production angle, using the H_8-beamline in the North Experimental Area as a charged-particle spectrometer (Fig.1).

The strangelets will be identified by the measurement of their rigidity R in the spectrometer, their velocity, and their charge. The velocity will be determined from the time-of-flight (TOF) measurements provided by TOF scintillation counter hodoscopes positioned along the beam spectrometer. A hadron calorimeter will be used to complement the momentum measurement with the spectrometer by an independent energy information, thus providing redundancy for effective background rejection. The interesting charge and mass range ($10 < m < 40$ GeV/c^2) of the strangelets can be covered quite effectively by two settings of the beam spectrometer with the rigidities R = 200 GV and R = 100 GV (Fig.9). Assuming a distance of 550 m between the production target and the last counters in the beam spectrometer, the strangelets should have a lifetime $\gamma\tau > 2 \cdot 10^{-6}$ s in order to be detected. It is the aim of the experiment to reach a detection sensitivity for strangelets of 10^{-9} to 10^{-10} per interaction.

We further propose to investigate particle production in relativistic heavy ion collisions with emphasis on antibaryon (antiproton, antideuteron) production by measuring their production yields over 2 units of rapidity each (Fig.15), and at production angles from 0 to 12 mrad. The particles will be identified by means of two CEDAR counters, one threshold Čerenkov counter, and by TOF measurements.

2. Physics motivation for the strangelet search

This experiment will look for new phenomena which have been predicted to occur in heavy ion collisions. As pointed out in Ref.[1-6], strangelets could be produced in a baryon-rich quark gluon plasma (QGP). If so, they will serve as an unique signature for the QGP formation. Their production is due to a cooling process of the plasma which results in a strong enhancement of the s-quarks in the quark phase. The cooling mechanism of the plasma is initiated by the evaporation of pions, K^+ and K^o, which carry entropy and antistrangeness away from the system. The strong s quark enhancement in the baryon-rich environment of the plasma then favours the formation of strangelets. In contrast to nuclear matter, strangelets consist of approximately the same

number of u, d, and s quarks. On the basis of the Pauli exclusion principle, such multiquark states become stable owing to the introduction of strangeness as an additional degree of freedom (Fig.2). A strangelet with baryon number A and total energy E is stable against strong decays if $E/A \leq M_n$ or M_Λ, the masses of the nucleon and Λ hyperon respectively. Even if E/A exceeds M_n, a strangelet would not disintegrate rapidly into nucleons, because the process would require several weak interaction processes. For sufficiently large A (A > 10), depending on the choice of the bag parameter, strangelets could be stable with respect to strong and weak nucleon emission. The lifetime of strangelets has been estimated in Ref.[7].

Strange matter can exist in charged and neutral form. Its charge-to-baryon-number ratio is $Z/A = (1-f_s)/2$, assuming equal numbers of u and d quarks. The quantity f_s is defined as the number of strange quarks per unit of A. It can have values >1, <1, and =1, leading to negative, positive and neutral charge states, respectively. Typical values of f_s between 0.5 and 1.0 might be expected [1,2]. This corresponds to Z/A values between 0 and 0.25. These rather small charge-to-mass ratios present a promising experimental signature. The existence of strangelets is not only of interest to nuclear and particle physics, but also to astrophysics, as was pointed out in Ref. [8,9]. Strangelets produced in a first-order phase transition in the early universe could also be candidates for dark matter. The great potential importance of such objects justifies careful searches.

Experimental searches for strange matter were recently carried out in heavy ion collisions at the AGS at Brookhaven (Experiment E814 [10] and E858 [11]) and in a cosmic-ray experiment [12]. The E814 results give an upper limit corresponding to a 90% confidence level of less than $1.2 \cdot 10^{-4}$ strangelets per interaction for multiply charged, and less than $8.3 \cdot 10^{-4}$ per interaction for singly charged strangelets. The cosmic ray experiment, however, reports two events which may be explained by the hypothesis of strange quark matter with Z ~ 14 and A ~ 350. The Brookhaven groups have been approved to continue their strangelet search with Au ion beams of 11.7 GeV/nucleon [E864, J. Sandweiss et al., and E878, H.J. Crawford et al.] which will become available in the near future. Our proposed experiment is complementary to the strangelet search program at Brookhaven, and is justified by the much higher ion beam energies available at CERN. There exists also another approach for a strangelet experiment at CERN (letter-of-intent I 183, P. Sonderegger et al.).

As pointed out in Ref.[13], strangelet searches could become very difficult if not impossible at heavy ion colliders such as the LHC, since the central rapidity regions are expected to be baryon-free, and strangelets can

only be produced in a baryon-rich environment. This again makes the SPS at CERN a more profitable hunting ground.

3. Antibaryon production in heavy ion collisions

Antibaryon production is of particular interest in heavy ion collisions. Most models assume that antibaryons arise via coalescence of three antiquarks, and are therefore sensitive to the thermal antiquark distributions and the chemically equilibrated antiquark abundances in the QGP. It was conjectured that high antiquark densities in the QGP might lead to antibaryon as well as antinucleus abundances [10,11]. However, baryon-antibaryon annihilations in the hadron gas may considerably dilute these abundances. Preliminary results from experiment E858 [11] with Si beams showed that the $\bar{p}$ and $\bar{d}$ yield at 0° production angle is significantly smaller than expected from coalescence models.

Our proposed focusing spectrometer experiment is well suited for a systematic study of antibaryon production in heavy ion collisions over a large rapidity range. The incident ion beam can be steered at an angle of maximally 12 mrad onto the production target. This allows us to study particle production at angles between 0 and 12 mrad. The region near 0 degrees and forward rapidities is not easily accessible to other heavy ion experiments at CERN. We will be able to measure particle production as a function of the transverse kinetic energy $T_T = m_T - m_o$ (where the transverse mass is $m_T = \sqrt{m_o^2 + p_T^2}$, and is m_o the rest mass of the particle) within a small T_T range. The covered transverse momentum range will be $0 < p_T < 0.120$ GeV/c at a particle momentum of 10 GeV/c, and with $0 < p_T < 1.26$ GeV/c at 105 GeV/c.

Using different targets like Al, Cu and Pb we will be able to study the amount of reabsorption of antiprotons and antideuterons as a function of the target mass.

4. Apparatus

We would like to use the H_8-beamline in the North Area of the SPS as a secondary beam spectrometer because of its large acceptance (4 μsr, $\frac{\Delta p}{p}$ = 6%). The beamline consists of a first section with a momentum focus, and a second clean-up section with an achromatic final focus. Originally this beamline had a parallel section for the insertion of CEDAR Cerenkov counters, which has since been removed. This section will have to be reinstalled, together with two CEDAR counters, for this experiment.

As sketched in Fig.1, the beam spectrometer will only be instrumented in the second section of the beam. For the velocity measurement of the strangelets, 4 TOF scintillation counter hodoscope layers (TOF_1 ... TOF_4), distributed along the beamline, will be used. This arrangement allows for two independent velocity measurements. The charge of the strangelets will be determined from the $\frac{dE}{dx}$ information of the TOF scintillation counters, as well as from the combination of the energy measurement in the hadron calorimeter, and the rigidity of the beam spectrometer. A wire chamber system (W_1 ... W_7) will be implemented to serve the following functions: a) To identify double or multiple tracks traversing the TOF counters; b) to improve the momentum resolution of the H_8-beam spectrometer, and c) to provide charged-particle tracking through the spectrometer. The rigidity of the strangelets will be measured by means of chambers W_1, W_2, W_3 and W_4 with a resolution of $\frac{\Delta p}{p} = \pm 10^{-3}$. The strangelet mass can then be determined from its charge, velocity and rigidity. A second mass determination can be obtained from the calorimeter energy and the velocity measurement. For this purpose we plan to use the compensating Uranium/scintillator test calorimeter of the ZEUS Collaboration. This calorimeter has been touched up, and was successfully used during our test beam run in September 1991. The calorimeter has the dimensions 60 x 60 cm^2 and is 7.1 λ thick. For the detection of π, K, p and d particles, two CEDAR (C_1, C_2), one threshold Cerenkov counter (C_3), and the TOF counters will be used. The incident ion beam will be monitored with a fast quartz counter. Central heavy ion collisions will be tagged by a fast multiplicity counter array which surrounds the production target.

The spectrometer is instrumented in such a way that the important parameters for the strangelet identification are measured with sufficient redundancy to suppress the background effectively.

a) TOF-scintillation counter hodoscopes

Four scintillation-counter hodoscopes are foreseen to provide the time-of-flight information of the particles in the spectrometer. They are positioned along the beamline at locations where the vacuum is interrupted due for the insertion of trigger counters (Trig1, Trig2 and Trig3) that are used for beam tuning purposes. The approximate distances between TOF_1 and TOF_2, TOF_2 and TOF_3, TOF_3 and TOF_4 are 90 m, 60 m, and 165 m, respectively. The distance between TOF_1 and TOF_4 is therefore approximately 315 m. TOF_1, TOF_2, and TOF_3 are identically constructed. Each hodoscope will cover the maximum beam aperture of 8.6 x 10 cm^2. Fast BICRON 404 scintillator strips with dimensions 10 cm x 3 cm x 0.5 cm (length x width x thickness) will be used.

The strips are slightly overlapping in the beam direction. Each scintillator is read out via a light guide and a phototube (Hamamatsu R1828-1) at both ends. TOF_4, positioned at the final focus of the beam, will consist of two scintillators with dimensions 4 x 2 x 1 cm^3. The scintillator will be read out on both ends. Vetocounters will be used to protect the light guides and PM's of the TOF hodoscopes.

A similar TOF hodoscope, build out of scintillator strips (BICRON 404) of dimensions 75 x 3 x 1 cm^3, was tested in September 1991. We obtained a time resolution of σ_t = 80 ps for minimum-ionizing particles (Fig.3). We believe that resolutions of σ_t ~ 60 ps can be achieved for the small-size scintillator strips proposed for our TOF counters. Time resolutions of σ_t ~ 55 to 57 ps have been measured with scintillators (BICRON 404) of the dimensions 20 x 1.6 x 0.6 cm^3 using Hamamatsu R3478 photomultipliers, by the NA44 collaboration [16].

We also measured a time resolution of σ ~ 38 ps with a small scintillator of dimensions 1 x 1 x 1 cm^3, which we used as a start counter in the September 1991 test beam run (Fig.4). A similar time resolution should be achievable for TOF_4.

b) Calorimeter

Fig.5 shows the dimensions, the segmentation and some details of the calorimeter structure. The overall sensitive dimensions covered by the scintillator and uranium material are 60 x 60 cm^2. To obtain compensation, the scintillator thickness was chosen to be 3 mm, while the uranium plates have a thickness of 3.2 mm. Each calorimeter module is segmented into 12 independent strips. The strips are read out via wavelength shifter light guides and phototubes at each end. In addition, a fifth module M_5 (not shown in Fig.5) will be used; it contains 5 mm-thick scintillators and 3.2 mm-thick uranium plates, corresponding to 1.0 λ. Its strip segmentation is identical to the other four modules. The total number of phototubes is 120. The hadronic energy resolution was measured to be

$$\frac{\sigma}{E} = \frac{0.35}{\sqrt{E}} \oplus 0.01 \quad [E \text{ in GeV}]$$

over a fiducial area of 20 x 20 cm^2 [ZEUS Calorimeter group 17]. The phototube signals of the calorimeter will be integrated during a gate time of 160 ns.

Since the fine segmentation of the ZEUS test calorimeter is an overkill for our purpose, we are presently investigating the possibility of either finding a suitable existing calorimeter (with a few individual cells only) or of constructing a new one.

c) Wire chambers

We are planning to use seven proportional wire chambers with digital readout. Each chamber is equipped with x and y planes. The wire spacing is 3 mm. The standard size of the chambers will be 110 x 110 mm^2 and covers the full beam aperture. For the high transmission mode of the H_8-beamline, the chamber W_2 has to be about a factor two larger in its vertical dimension in order to account for the large beam momentum dispersion of 26 mm per $\frac{\Delta p}{p} = 0.01$. The wire chamber system provides excellent momentum resolution $\left[\frac{\Delta p}{p} \sim 10^{-3}\right]$ as well as tracking for secondary particles in the beam spectrometer.

d) Target box

The target box located just upstream of the T_4 proton target fits in a space of 6 cm in the beam direction. It contains the incident beam detector, various production targets (which can be moved into the beam by remote control) and the multiplicity counters (Fig.6). For the incident beam detector, which has to operate at $5 \cdot 10^7$ ions/spill, we will use the design of the NA 38 experiment. It consists of a 3 mm thick quartz Čerenkov counter with an optical-fiber light collection system. Downstream of the production target, four additional quartz Čerenkov counters measure the multiplicity of the event. Note that this is strongly correlated with the centrality of the interaction.

e) Trigger and data acquisition

The fast constant-fraction discriminators of the TOF counters will be located close to these counters in order to avoid a slowing down of the phototube signals by long cables. The discriminator signals will be refreshed by means of ultra-fast comparators at the inputs of the time-to-charge converters which are installed in the CAMAC crates in the electronics hut near the end of the beam line. Times and pulse heights will be digitized by FERA ADC's (LeCroy 4300). The first-level trigger will be derived from the TOF hodoscope and from additional beam counters at the end of the beam line. The

TOF start and ADC gate signals will be adequately delayed by means of cables.

A schematic diagram of the hardware configuration planned for data acquisition (DAQ) is shown in Fig.7. Three CAMAC crates with FERA ADC's digitize the signals from the calorimeter from TOF hodoscopes 1 and 4, and from TOF hodoscopes 2 and 3, respectively. A second-level trigger module (see next paragraph) will be located in the same crate as the ADC's, for TOF planes 1 and 4. The data from those ADC's will be transferred to the second-level trigger module through the fast ECL ports. For events to be rejected, the second-level trigger produces a fast clear for all ADC's. For accepted events, the second-level trigger module transfers the data obtained from the ADC's over a fast (~ 200 ns / 16 bit word) differential ECL bus into a commercial (HSM 8170 from CES) high-speed memory of 1 MB capacity, which sits in a VME crate. The data from the ADC's in the other crates will be transferred in the same way directly to corresponding VME memory modules. The maximum event rate thus achievable is limited by the capacity of the VME memory modules. Given that there are 120 channels/event from the calorimeter, we can accumulate ~ 4000 events/spill, or ~ 720'000 events/hour, assuming an SPS cycle time of 20 sec, with only a few percent dead time. In principle, this limit could be pushed even further by increasing the size of the memory (by cascading several modules on the same ECL bus), but the resulting data volume would soon become inpracticable.

The data acquisition process will be controlled from an MVME167 CPU-module sitting in the same VME crate as the high-speed memory modules. Between SPS-bursts, the data from the memories will be collected reformated, and written on EXABYTE 8 mm cartridges (maximum transfer rate = 0.5 MB/sec, or 10 MB per SPS (super-)cycle).

The microprocessor will be running Microware's OS9 operating system. All software will be written in the framework of the SPIDER data acquisition system provided by the CERN ECP-DS group. Our group has successfully used SPIDER and OS9 in a test beam experiment in 1991.

f) Second-level trigger

Data accepted by the first-level trigger will be partially read out by a specially designed second-level trigger system. This system uses the time and pulse height information from the two extreme TOF hodoscopes (TOF_1 and TOF_4). Events with pulse heights compatible with $Z \geq 2$ will be accepted regardless of their time of flight information. The rest of the events will be selected according to their time-of-flight information. The trigger decision, which constitutes a mass cut, will be available approximately 5 μs after the last

data have been read, or 26 μs after first-level trigger acceptance. It will then enable a full readout of the data, or provide a fast clear to the system.

The high processing speed is made possible by the pipeline architecture chosen for the system. Since the amplitude as well as the time information is recorded for each timing channel, the digitized data will consist of time and amplitude pairs. These will be digitally corrected for pedestal and calibration constants in a trigger processor input channel. In the first and last timing plane, the two timing values corresponding to the opposing photomultiplier pair with the highest amplitudes, are averaged. The two averages are then subtracted, comparing the result to internally stored limit values, to obtain the desired mass cut. The data used by the trigger will also be buffered in an internal memory so that they can be included on tape, should the event be accepted (Fig.8).

The trigger processor is based on a CAMAC module containing programmable gate arrays, random access memories and fast 12-bit multipliers. A range of modifications of the trigger algorithm can be directly implemented by altering the configuration information sent to the gate arrays during system initialization. This also includes the possibility to use special test and diagnostic configurations for maintenance. This solution has the advantage of flexibility as well as serviceability.

5. Spectrometer acceptance

We assume that the strangelets are produced with a momentum and rapidity distribution in the center of mass (C.M.S) [7], which we will parameterize

$$\frac{d^2N}{dy\,dp_T} = \frac{p_T}{\bar{p}_T^{\,2}} \cdot e^{-p_T/\bar{p}_T} \cdot \frac{1}{\sqrt{2\pi}\ \sigma_y} \cdot e^{-(y-\bar{y})^2/2\sigma_y^2} .$$

Here y is the rapidity, $\bar{y}$ is the laboratory rapidity of the C.M.S, p_T is the transverse momentum, $\bar{p}_T$ = 1/2 $\langle p_T \rangle$, $\langle p_T \rangle$ is the average transverse momentum, and σ_y the width of the rapidity distribution. In Pb-Pb collisions at 160 GeV/nucleon incident energy, $\bar{y}$ is 2.9. The average transverse momentum is not known. In the following, we assumed a value $\langle p_T \rangle$ = 0.5 $\sqrt{m}$ GeV/c, where m is the mass of the strangelet. The average transverse momentum of the strangelets can, however, be much smaller, in particular if QGP cooling leads to heavy mass strangelets. In this case, the spectrometer acceptance α is even larger (Fig.9). The width of the rapidity distribution was assumed to be

σ_y = 0.5. After the variable transformation (y, p_T) → (p, θ) we can calculate the strangelet acceptance α in the focusing spectrometer. Fig.10 shows the acceptance α/Z of the H_8-beam spectrometer versus m/Z, with Z the charge of the strangelet, for 0° production angle, and for spectrometer rigidities R = 200 GV, 150 GV, 100 GV, and 50 GV. For numerical values, see also Table 1. If we assume $\langle p_T \rangle = 0.1 \sqrt{m}$ GeV/c, the spectrometer acceptances in Table 1 are by a factor 25 larger. Simple model calculations show that the most likely strangelet masses produced in Pb-Pb collisions with 160 GeV/nucleon incident energy are smaller than 40 GeV/c^2. Fig.10 shows that the mass range 5 < m < 40 GeV/c^2 is well covered with the two spectrometer rigidity settings R = 100 GV and R = 200 GV.

Table 1

The acceptance α of the H_8-spectrometer is shown for various strangelet masses m, strangelet charges Z, and spectrometer rigidities. Also shown are the rapidities y. A production angle of 0° and $\langle p_T \rangle = 0.5 \sqrt{m}$ GeV/c was assumed.

			rigidities		
Z/m	m	Z	50 GV	100 GV	200 GV
			y = 3.0	y = 3.7	y = 4.4
0.2	5	1	$2.2 \cdot 10^{-4}$	$2.5 \cdot 10^{-4}$	$3.7 \cdot 10^{-5}$
	10	2	$4.5 \cdot 10^{-4}$	$4.9 \cdot 10^{-4}$	$7.4 \cdot 10^{-5}$
	20	4	$8.9 \cdot 10^{-4}$	$9.8 \cdot 10^{-4}$	$1.5 \cdot 10^{-4}$
	40	8	$1.8 \cdot 10^{-3}$	$2.0 \cdot 10^{-3}$	$3.0 \cdot 10^{-4}$
			y = 2.3	y = 3.0	y = 3.7
0.1	10	1	$5.7 \cdot 10^{-5}$	$4.3 \cdot 10^{-4}$	$4.6 \cdot 10^{-4}$
	20	2	$1.1 \cdot 10^{-4}$	$8.7 \cdot 10^{-4}$	$9.3 \cdot 10^{-4}$
	30	3	$1.7 \cdot 10^{-4}$	$1.3 \cdot 10^{-3}$	$1.4 \cdot 10^{-3}$
	40	4	$2.3 \cdot 10^{-4}$	$1.7 \cdot 10^{-3}$	$1.9 \cdot 10^{-3}$
			y = 1.9	y = 2.6	y = 3.3
0.067	15	1	$1.1 \cdot 10^{-5}$	$2.5 \cdot 10^{-4}$	$8.3 \cdot 10^{-4}$
	30	2	$2.2 \cdot 10^{-5}$	$4.9 \cdot 10^{-4}$	$1.7 \cdot 10^{-3}$
	45	3	$3.3 \cdot 10^{-5}$	$7.4 \cdot 10^{-4}$	$2.5 \cdot 10^{-3}$
			y = 1.65	y = 2.3	y = 3.0
0.05	20	1	$2.4 \cdot 10^{-6}$	$1.1 \cdot 10^{-4}$	$8.3 \cdot 10^{-4}$
	40	2	$4.7 \cdot 10^{-6}$	$2.2 \cdot 10^{-4}$	$1.7 \cdot 10^{-3}$

6. Rates and Sensitivities for the strangelet search

We assume an incident beam intensity of $5 \cdot 10^7$ ions per burst. The burst length is 5 s, the SPS cycle time 19.2 s. We propose to use a 4 cm Pb target, corresponding to 1 interaction length. Under these conditions we expect N_i = $6.3 \cdot 10^6$ interactions per second during the spill.

To estimate the trigger rate in our detector, we used the FRITIOF program to generate events in Pb-Pb collisions. We expect at 0° production angle, with a spectrometer rigidity R = 200 GV and positive polarity, $1.7 \cdot 10^{-2}$ particles (mostly protons) per interaction in the H_8-spectrometer. For the same rigidity and negative polarity, the number is $1.6 \cdot 10^{-4}$ particles per interaction. This corresponds to an instantaneous rate of 10^5particles/s for positive polarity, and 10^3particles/s for negative polarity. The corresponding numbers for the spectrometer rigidity R = 100 GV are $1.8 \cdot 10^5$/s and 10^4/s for positive and negative beam polarities, respectively (see also Table 4). This rate will be reduced by about a factor 10^2 through an effective threshold Čerenkov counter veto, which rejects protons, kaons and pions. As we described earlier, a second-level trigger processor will be used for data reduction. The surviving high-mass events will be recorded on tape.

We define the detection sensitivity s for strangelets to be

$$s = \frac{N_e(m)}{N_a \cdot \alpha \cdot \varepsilon} \quad ;$$

here, N_a is the total number of primary interactions, α is the acceptance of the beam spectrometer, and ε the detection efficiency. $N_e(m)$ is the number of detected events needed to claim a signal above background, in a mass region corresponding to the detector resolution. In the following, we assume a negligible background ($N_e(m) = 1$).

We propose to take data with spectrometer rigidities R = 200 GV, 100 GV each, with positive and negative beam polarities. If we assume 8 days running for each of these settings, we will end up with 32 days of data taking. In addition we need 4 days of setup time prior to data taking, and a total of 2 days for changing between the various beam settings. This results in a total of 38 days of beam time, corresponding to about one year ion beam operation of the SPS. For 8 days (corresponding to $7 \cdot 10^5$ s) of data taking, assuming $5 \cdot 10^7$ ions/spill and an overall beam time efficiency of $\varepsilon_b = 0.5$, we expect to have a total number of primary interactions on a 1 λ Pb target of N_a = $5.7 \cdot 10^{11}$.

Fig. 11 shows the detection sensitivity for strangelets at 0° production angle, with $\langle p_T \rangle = 0.5 \sqrt{m}$ GeV/c, for spectrometer rigidities of R = 200,

100, and 50 GV, under the assumption of a detection efficiency $\varepsilon = 1$. Assuming that strangelets interact like nuclei with matter, we estimated their detection losses due to interactions within the production target and with materials in the beam line (scintillator, vacuum windows, Čerenkov counters, wire chambers, and air). For a strangelet mass of $m = 10$ GeV/c^2, we obtain a detection efficiency $\varepsilon = 2/3$. As an example, the strangelet detection sensitivities for rigidity $R = 100$ GV and for $N_a = 5.7 \cdot 10^{11}$ primary interactions, are shown in Table 2. Here, strangelet absorption has been taken into account.

Table 2

Strangelet detection sensitivities for a rigidity of $R = 100$ GV and $N_a = 5.7 \cdot 10^{11}$ primary interactions, corresponding to 8 days of beam time. The strangelet absorption in materials is taken into account.

mass of strangelet GeV/c^2	Z	strangelet detection sensitivities assuming $\langle p_T \rangle = 0.5 \sqrt{m}$	strangelet detection sensitivities assuming $\langle p_T \rangle = 0.1 \sqrt{m}$
$m = 10$	1	$6.2 \cdot 10^{-9}$	$2.5 \cdot 10^{-10}$
$m = 20$	2	$3.3 \cdot 10^{-9}$	$1.3 \cdot 10^{-10}$
$m = 30$	3	$2.4 \cdot 10^{-9}$	$9.6 \cdot 10^{-11}$
$m = 40$	4	$2.0 \cdot 10^{-9}$	$8.0 \cdot 10^{-11}$

The mass resolution of strangelets at high energies is dominated by the accuracy of the time-of-flight measurements. In our calculations, we assume a time resolution of $\sigma_t \sim 80$ ps for each of the TOF_1, TOF_2 and TOF_3 counters, and $\sigma_t \sim 40$ ps for the TOF_4 counter. These time resolutions correspond to the values we obtained with similar counters as shown in Fig.3 and 4. A linear fit to the individual time measurements of all TOF-counters yields a total timing resolution of $\sigma_t = 78$ ps. For a total drift length of 315 m, we obtain

$\sigma_t/t = 7.4 \cdot 10^{-5}$. With a momentum resolution for the beam spectrometer of $\sigma_p/p = 0.85 \cdot 10^{-3}$, using the information of the wire chambers W_1, W_2, W_3, W_4, we can calculate the mass resolution of the strangelets from the relation

$$\sigma_m = \sqrt{\left(m \frac{\sigma_p}{p} \right)^2 + \left(\frac{\sigma_t}{t} \frac{E^2}{m} \right)^2} \quad .$$

E is the energy of the strangelet. A similar expression leads to the mass resolution if we consider the energy resolution of the hadron calorimeter σ_E/E

$$\sigma_m = \sqrt{\left(m \frac{\sigma_E}{E} \right)^2 + \left(\frac{\sigma_t}{t} \frac{E^2}{m} \right)^2} \quad .$$

As an example, the mass resolution σ_m obtainable with the beam spectrometer compared to two different hadron calorimeters with the resolutions

$$\frac{\sigma_E}{E} = \frac{0.35}{\sqrt{E}} \oplus 1\% \quad \text{and} \quad \frac{\sigma_E}{E} = \frac{0.5}{\sqrt{E}} \oplus 1\%$$

for rigidities R = 200 GV and R = 100 GV, are listed in Table 3. The mass resolutions σ_m as a function of m/Z for different spectrometer rigidities, are also shown in Fig.12.

In order to estimate the background due to protons, which are the dominating particles when running with positive polarity, we simulated the detector response assuming purely Gaussian distributions of the TOF counter time resolutions. Fig.13 and Fig.14 show the mass distributions of protons at rigidities R = 100 GV and R = 200 GV, respectively. The number of protons is normalized to $5.7 \cdot 10^{11}$ Pb-Pb collisions using the proton yields obtained from the FRITIOF simulations. Our quoted sensitivity for strangelet detection with masses above 4 GeV/c^2, will not be affected by proton background, as long as the time resolutions do not deviate from a Gaussian behaviour.

Table 3

Mass resolution σ_m obtainable with a TOF resolution $\sigma_t/t \sim 7.4 \cdot 10^{-5}$, a beam spectrometer resolution $\sigma_p/p = 0.85 \cdot 10^{-3}$, and two different hadron calorimeter resolutions $\sigma_E/E = 0.35/\sqrt{E} \oplus 1\%$, and $\sigma_E/E = 0.5/\sqrt{E} \oplus 1\%$.

Strangelet mass [GeV/c^2]	Strangelet momentum [GeV/c]	charge Z	Spectrometer + TOF σ_m [GeV/c^2]	Calorimeter + TOF σ_m [GeV/c^2] $\frac{\sigma_E}{E} = \frac{0.35}{\sqrt{E}} \oplus 1\%$	Calorimeter + TOF σ_m [GeV/c^2] $\frac{\sigma_E}{E} = \frac{0.5}{\sqrt{E}} \oplus 1\%$
rigidity R = 200 GV					
m = 10	200	1	0.30	0.40	0.47
m = 20	400	2	0.59	0.72	0.80
m = 30	600	3	0.89	1.03	1.12
m = 40	800	4	1.19	1.35	1.43
rigidity R = 100 GV					
m = 10	100	1	0.08	0.37	0.52
m = 20	200	2	0.15	0.55	0.75
m = 30	300	3	0.23	0.71	0.94
m = 40	400	4	0.30	0.86	1.12

7. Rates for the particle search

To keep the secondary interactions in the target material at a low level, we propose to use a 3% λ thick Pb target. Assuming an incident ion beam intensity of $5 \cdot 10^7$ ions/spill, we obtain an interaction rate of $N_i = 3 \cdot 10^5$ interactions/s during a 5 s spill. Using the FRITIOF simulations, as shown in Table 4, we estimate a maximum trigger rate of $8.4 \cdot 10^3$/s in the positive beam and $1.2 \cdot 10^3$/s in the negative beam. The event rate, however, can be reduced by prescaling majority particles in the beam.

We propose to take data at beam momenta 10, 17, 28, 53, and 105 GeV/c, with positive and negative polarities, at 0, 6, and 12 mrad production angle. Fig.15 shows the covered rapidity range for different particles. The transverse energy range covered for $\bar{p}$ is $T_T = 0$ - 7.64 MeV at 10 GeV/c and $T_T = 0$ - 585 MeV at 105 GeV/c. The corresponding transverse momentum range is $0 < p_T < 120$ MeV/c, at 10 GeV/c, and $0 < p_T < 1.26$ GeV/c, at 105 GeV/c.

To check the amount of antibaryon reabsorption at central and foreward rapidities as a function of the target mass we propose to measure the positive and negative particle yields at 10 GeV/c and 105 GeV/c with two additional targets, probably Al and Cu.

Table 4

Particle yields at 0° production angle per minimum-bias Pb-Pb collision, from FRITIOF Monte Carlo simulations are shown. The H_8-beam spectrometer acceptance and particle decays along the beam are taken into account.

momentum p [GeV/c]	$\bar{p}$	p	π^+ or π^-	K^+	K^-
10	$8.6 \cdot 10^{-5}$	$2.0 \cdot 10^{-4}$	$7.8 \cdot 10^{-4}$	$1.3 \cdot 10^{-7}$	$1.1 \cdot 10^{-7}$
17	$1.8 \cdot 10^{-4}$	$5.8 \cdot 10^{-4}$	$2.2 \cdot 10^{-3}$	$5.8 \cdot 10^{-6}$	$3.9 \cdot 10^{-6}$
28	$3.0 \cdot 10^{-4}$	$3.0 \cdot 10^{-3}$	$4.0 \cdot 10^{-3}$	$4.6 \cdot 10^{-5}$	$2.7 \cdot 10^{-5}$
53	$2.0 \cdot 10^{-4}$	$1.0 \cdot 10^{-2}$	$3.5 \cdot 10^{-3}$	$2.0 \cdot 10^{-4}$	$7.7 \cdot 10^{-5}$
105	$5.0 \cdot 10^{-6}$	$2.8 \cdot 10^{-2}$	$1.3 \cdot 10^{-3}$	$1.2 \cdot 10^{-4}$	$3.0 \cdot 10^{-5}$
200	-	$1.7 \cdot 10^{-2}$	$1.6 \cdot 10^{-4}$	-	-

The particles will be identified by means of Čerenkov counter and TOF measurements. At and below 28 GeV/c $\bar{p}$, and $\bar{d}$ will be selected by TOF measurements (Fig.16 and Fig.17). At and above 53 GeV/c, CEDAR and threshold Čerenkov counters will be used to measure the particle yields.

The centrality of the interaction will be tagged by the information of the multiplicity counters near the production target. FRITIOF simulations show that the particle yields increase by about a factor 3 for central collisions.

Assuming one day of data taking, we expect for $N_a = 3.36 \cdot 10^9$ ion interactions in the production target about $3 \cdot 10^5$ $\bar{p}$, at 10 GeV/c, and at 0° production angle. If the yield of $\bar{d}$ is as low as measured at the AGS, $\bar{d}/\bar{p} \sim 10^{-5}$, we would to have a run for at least 10 days to obtain a reasonable $\bar{d}$ signal. For the other momenta we propose to run approximately 1 day per momentum, per polarity and per production angle. This adds up to about 30 days of data taking. For the antibaryon reabsorption checks with Al and Cu targets, we need 6 days. In addition to this, we need a total of 4 days for setting up and for changing beam momenta and Čerenkov counter settings.

8. Beam time requests

Before taking data with Pb beams, we need 16 days in the H_8-beam line with incident protons from the SPS to calibrate the calorimeter, to adjust the pulse height and the timing of the TOF counters and to recommission the CEDAR counters.

For the strangelet search, we request 32 days of Pb beam with an intensity of $5 \cdot 10^7$ ions/spill for data taking. They are divided into 4 portions of 8 days each for running with 2 spectrometer rigidities (R = 200 and 100 GV) and two spectrometer polarities. Prior to data taking, we need 4 days for setting up, and 2 days for changing between the various beam settings. This adds up to a total of 38 days of beam time.

For the particle search, we request 36 days of data taking, with an incident Pb beam intensity of $5 \cdot 10^7$ ions/spill. This period will be used to measure positively and negatively charged particle yields at 5 different momenta and at 3 different production angles, and the reabsorption of $\bar{p}$ and $\bar{d}$. In addition, we need a 4 days for setting up and for changing beam momenta and Čerenkov counter settings.

9. Cost estimate

We estimate the cost for new equipment in kSFr. (1992) as follows:

Calorimeter:	
photomultipliers	48
movable support table	70
HV-system	66
TOF counters:	
mechanics	20
5 FERA-ADC's	25
discriminator components	30
Wire chambers	45
Target box and controls	30
Second level trigger	20
Cables	50
total	404 kSFr.

10. Request from CERN

We request that CERN reinstall the parallel section of the H_8-beam line. This is necessary for the insertion of the two CEDAR counters needed for the particle search. We further request that CERN provide the beam instrumentation, which consists of two CEDAR's and one threshold Cerenkov counter. For the wire chambers, we ask CERN to provide the gas supply system as well as the mechanical supports in the beam line. We would like to ask CERN also to provide the cables needed for the target box counters, the TOF counters and the wire chambers to the electronic hut. Some of these cables were laid out for the test in the H_6-beam, and can be reused. For the additional cabling, we estimate a cost of approximately 50 kSFr.

References:

[1] E. Fahri and R.L. Jaffe, Phys. Rev. D30, 2379, (1984)

[2] G. Greiner, D.H. Rischke, H. Stöcker, P. Koch, Phy. Rev. D38, 2797, (1988)

[3] H.W. Barz, B.L. Friman, J. Knoll and H. Schulz, Phys. Lett. B242, No. 3,4, 328, (1990)

[4] R.L. Jaffe, Phys. Rev. Lett. 38, 195, (1987) and 38, 1617 E, (1977)

[5] C.B. Dover, P. Koch, M. May, Phys. Rev. C40, 115, (1989)

[6] G.L. Shaw et al., Nature 337, (1989), 463

[7] H.J. Crawford, M.S. Desai and G.L. Shaw, UCI preprint, submitted to Phy. Rev. D

[8] E. Witten, Phys. Rev. D30, N2, 272, (1984)

[9] A. de Rujula, S.L. Glashow, Nature 312, 734, (20/27 Dec. 1984)

[10] J. Barrette et al., preprint BNL-43697, OG-2002

[11] H.J. Crawford et al., preprint to be published in the proceedings of the workshop on Strange Quark Matter in Physics and Astrophysics, Aarhus, Denmark, May 1991

[12] T. Saito et al., Phys. Rev. Lett. 65, N17, 2094, (1990)

[13] U. Heinz, P. Koch, B. Friman, Proceedings of the Large Hadron Collider Workshop, Aachen 4-9 Oct. 1990, Vol. II, page 1079

[14] J. Ellis, U. Heinz and H. Kowalski, Phys. Lett. B233, N1,2, (1989), 223-230

[15] C. Dover, U. Heinz, E. Schnedermann, J. Zimanyi, Phys. Rev. C44, N4, (1991), 1636-1654

[16] T. Kobayashi and Sugitate, preprint June 1989

[17] G. D'Agostini et al., NIM A274, 134, (1989)

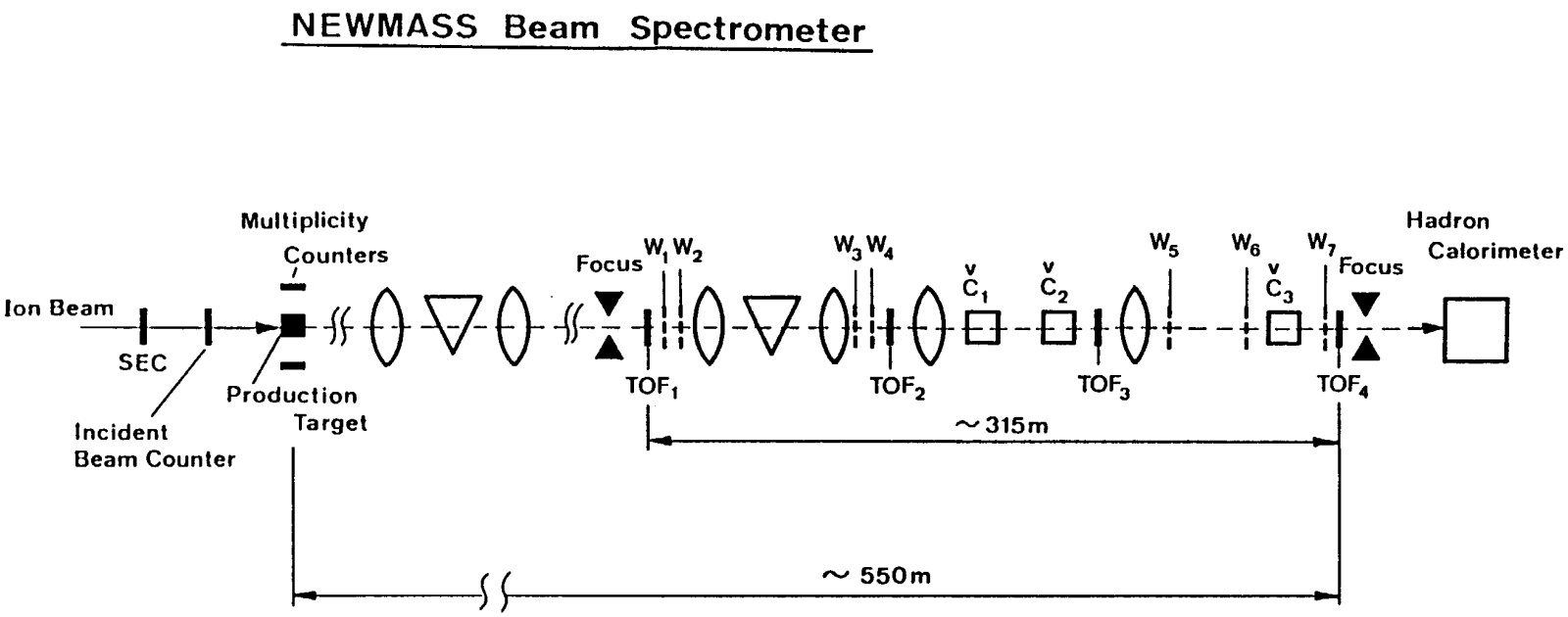

Fig.1 Schematic layout of the experiment

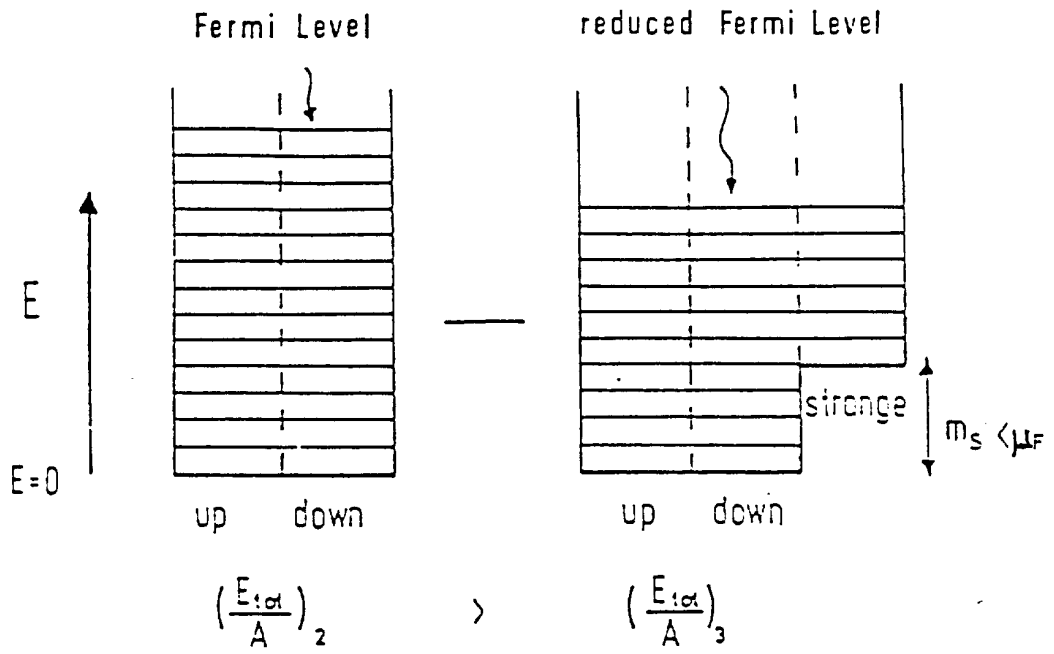

Fig.2 Schematic model for the reduction of the Fermi energy levels in a hadron or QGP bag due to the opening of an additional flavour degree of freedom.

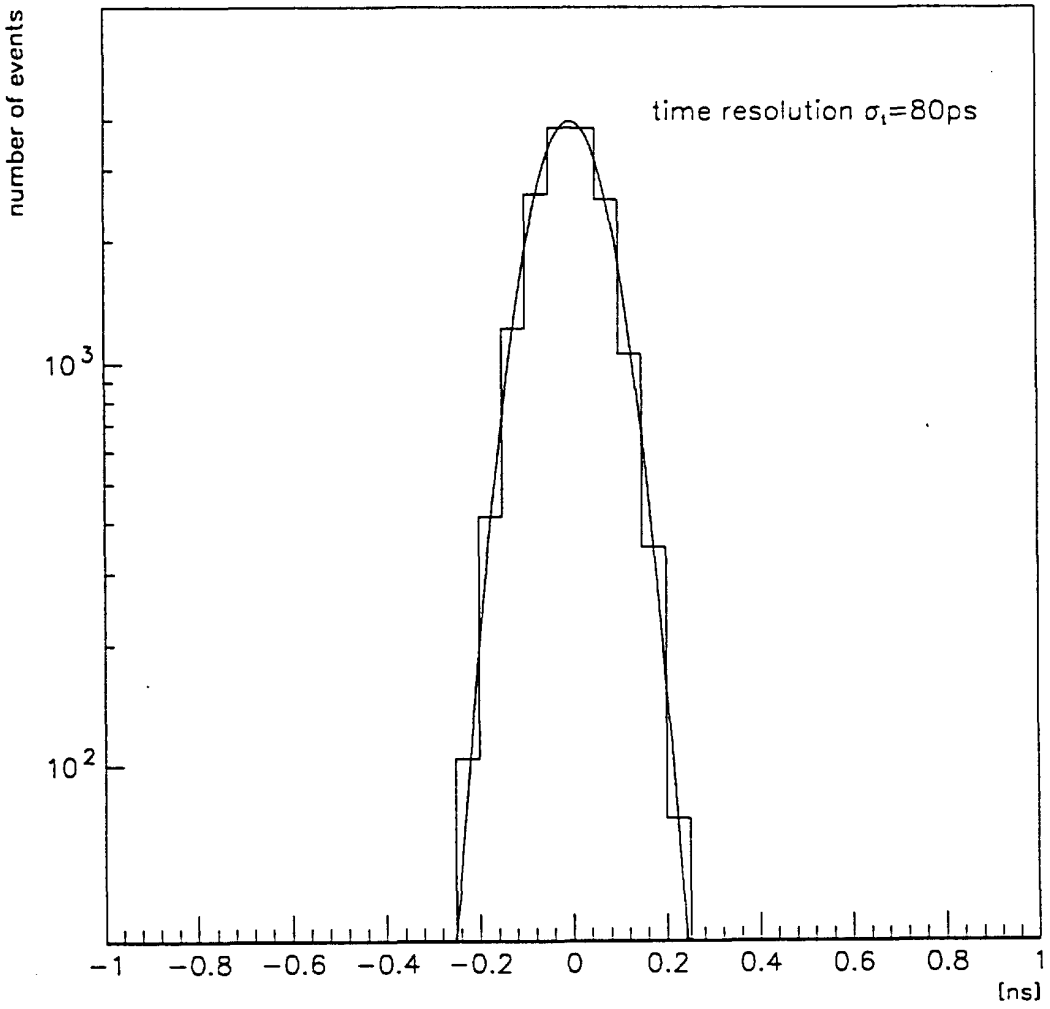

Fig.3 The measured time resolution for minimum-ionizing particles traversing a 75 cm long, 3 cm wide and 1 cm thick scintillation counter (BICRON 404) viewed at each end by a Hamamatsu R1828-1 photomultiplier (PM1 and PM2) is shown. The resolution is defined as $\sigma_t = \sqrt{\frac{\sigma_t^2\ (PM1) + \sigma_t^2(PM2)}{4}}$.

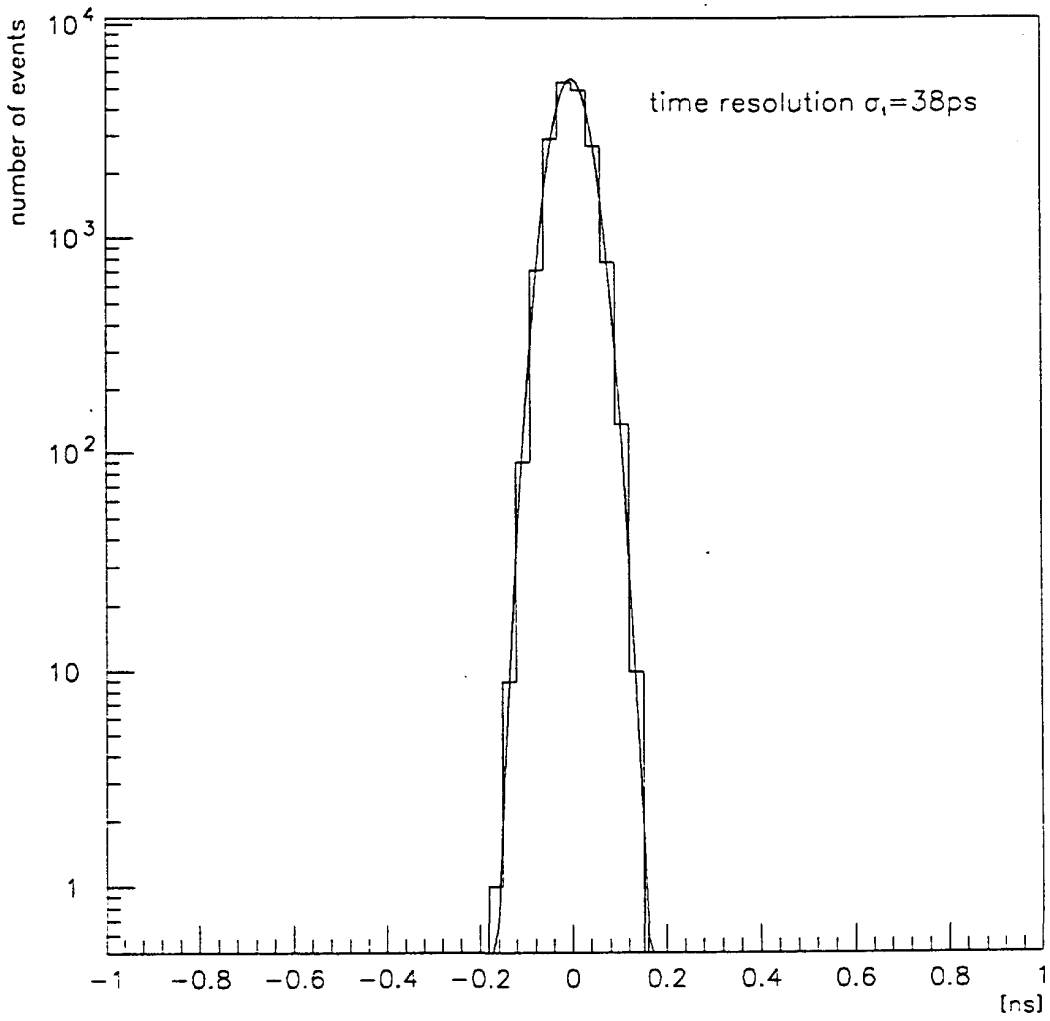

Fig.4 The measured time resolution for minimum-ionizing particles traversing a 1 cm x 1 cm x 1 cm scintillator (BICRON 404) viewed at each end by a Hamamatsu R1828-1 photomultiplier (PM1 and PM2) is shown. The resolution is defined as $\sigma_t = \sqrt{\frac{\sigma_t^2\,(\mathrm{PM1}) + \sigma_t^2(\mathrm{PM2})}{4}}$.

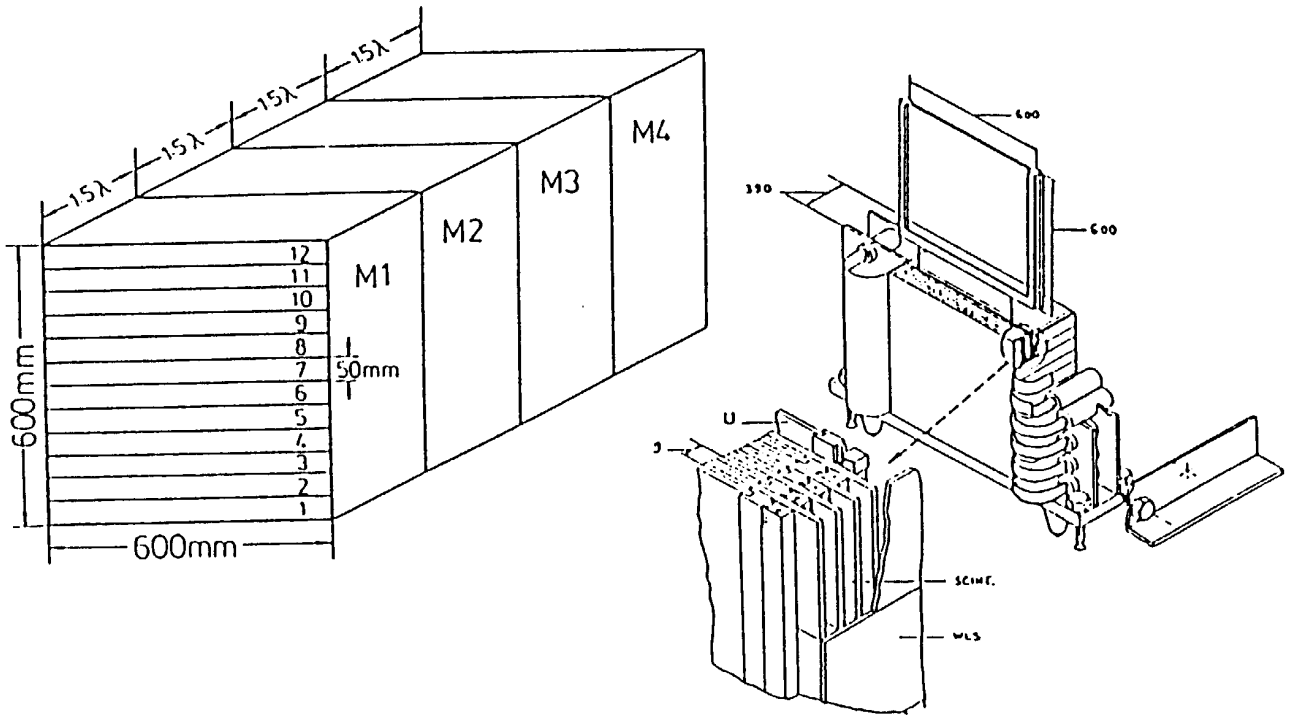

Fig.5 The uranium scintillator calorimeter with details of the layer structure.

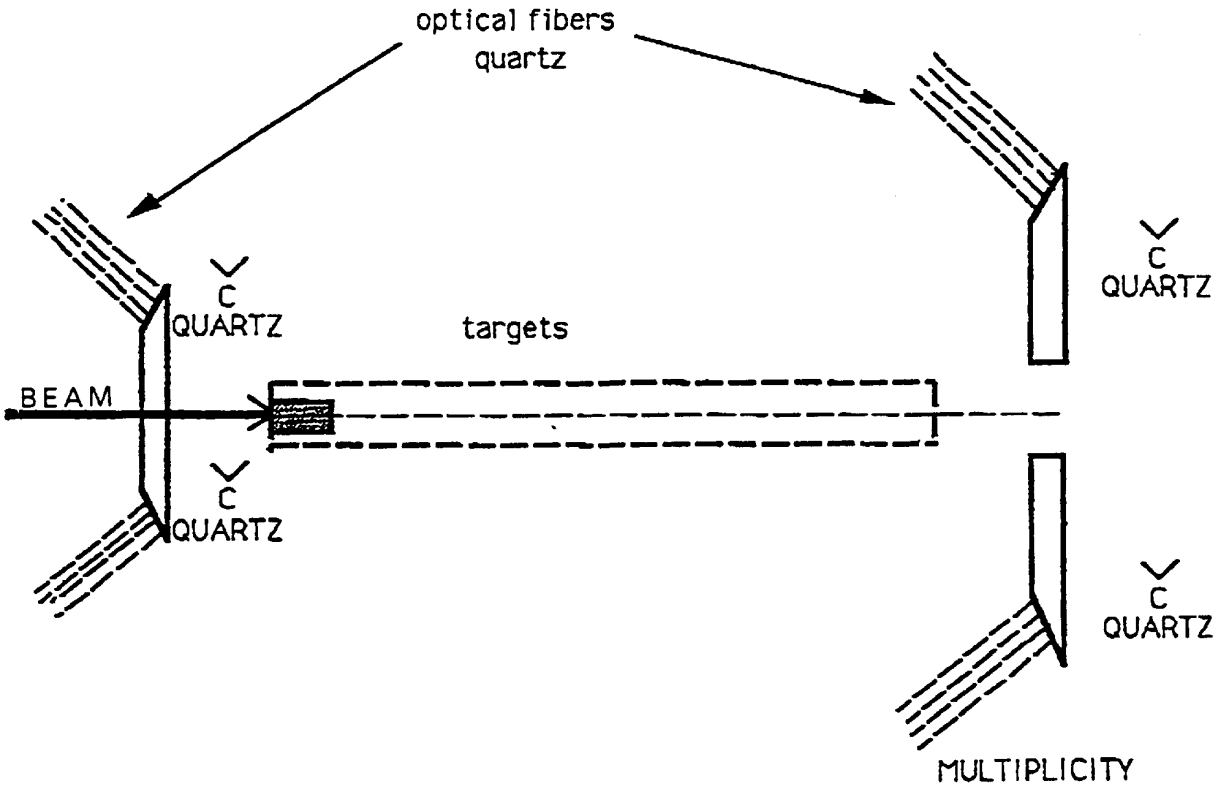

Fig.6 Schematic view of the target box.

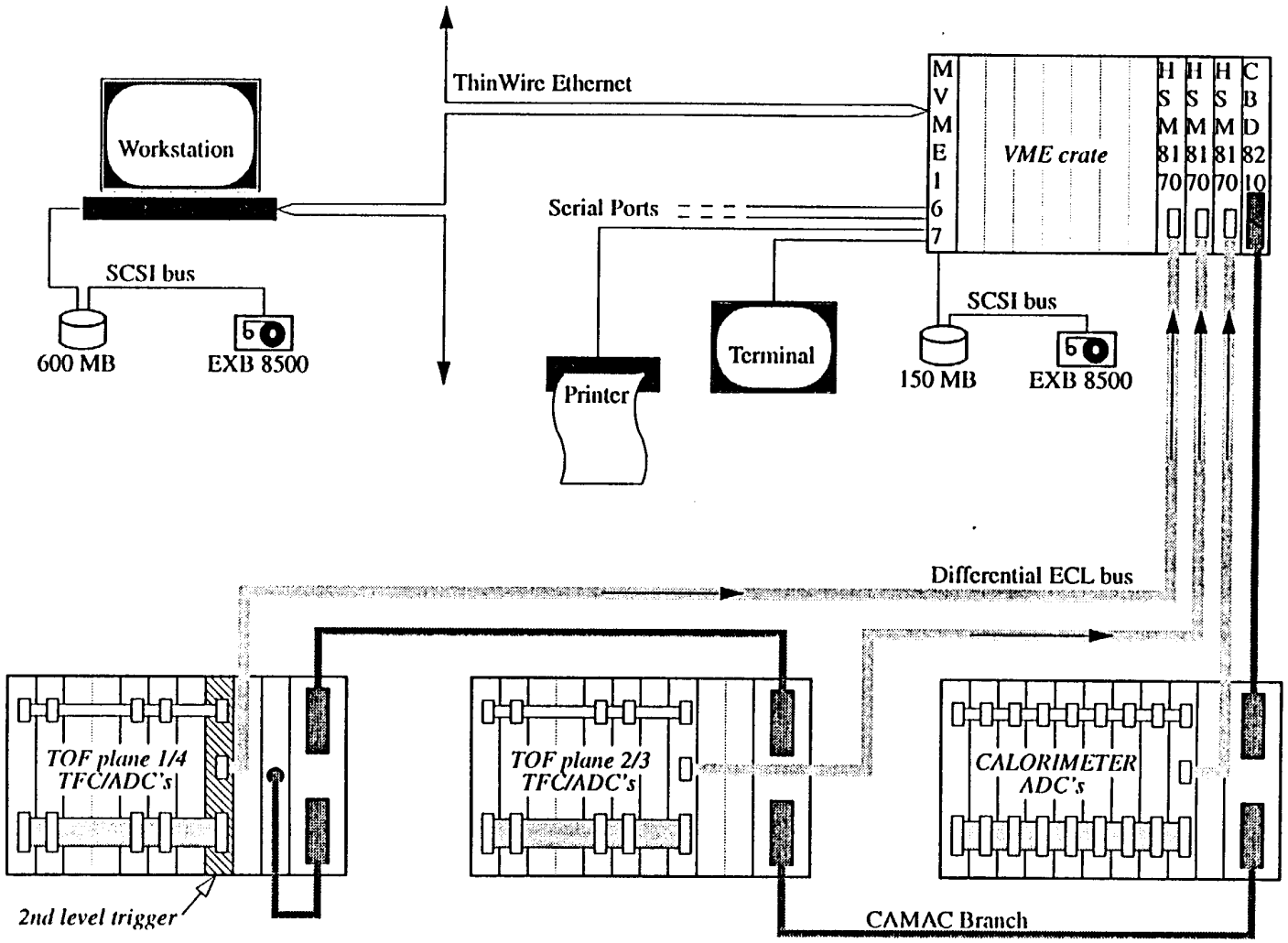

Fig.7 Schematic diagram of the hardware configuration planned for data acquisition.

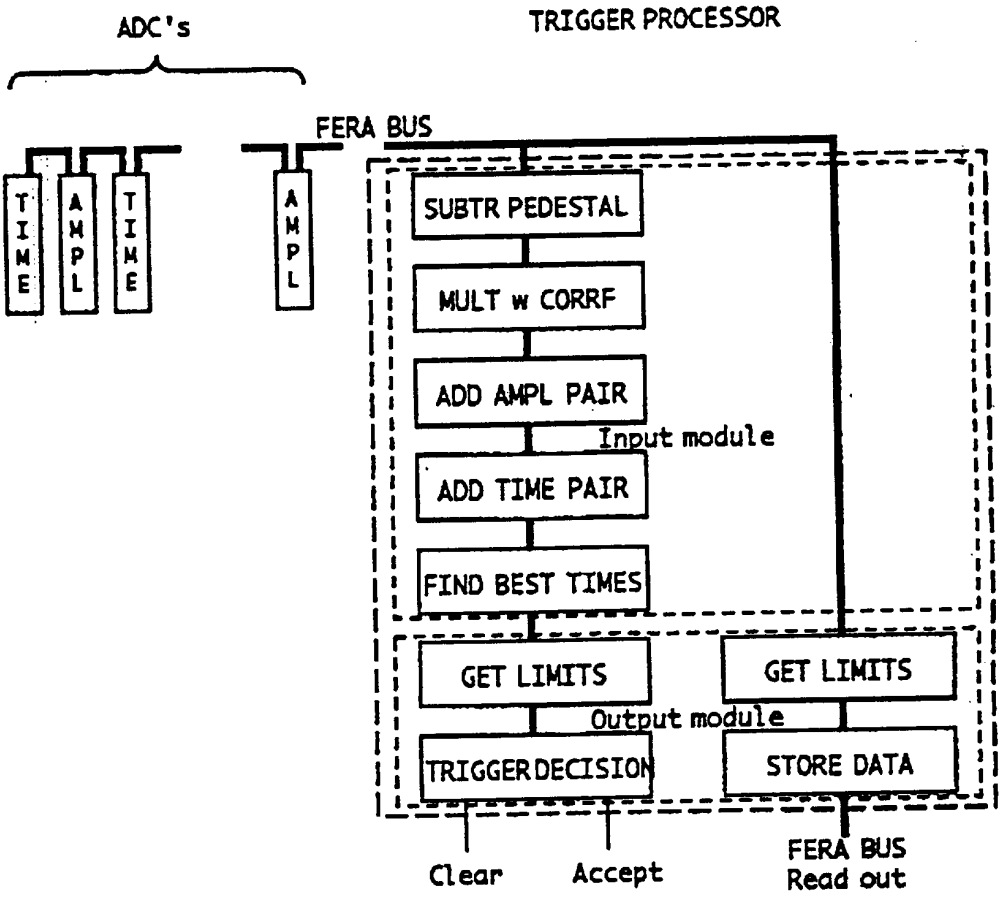

Fig.8 Schematics of the trigger processor.

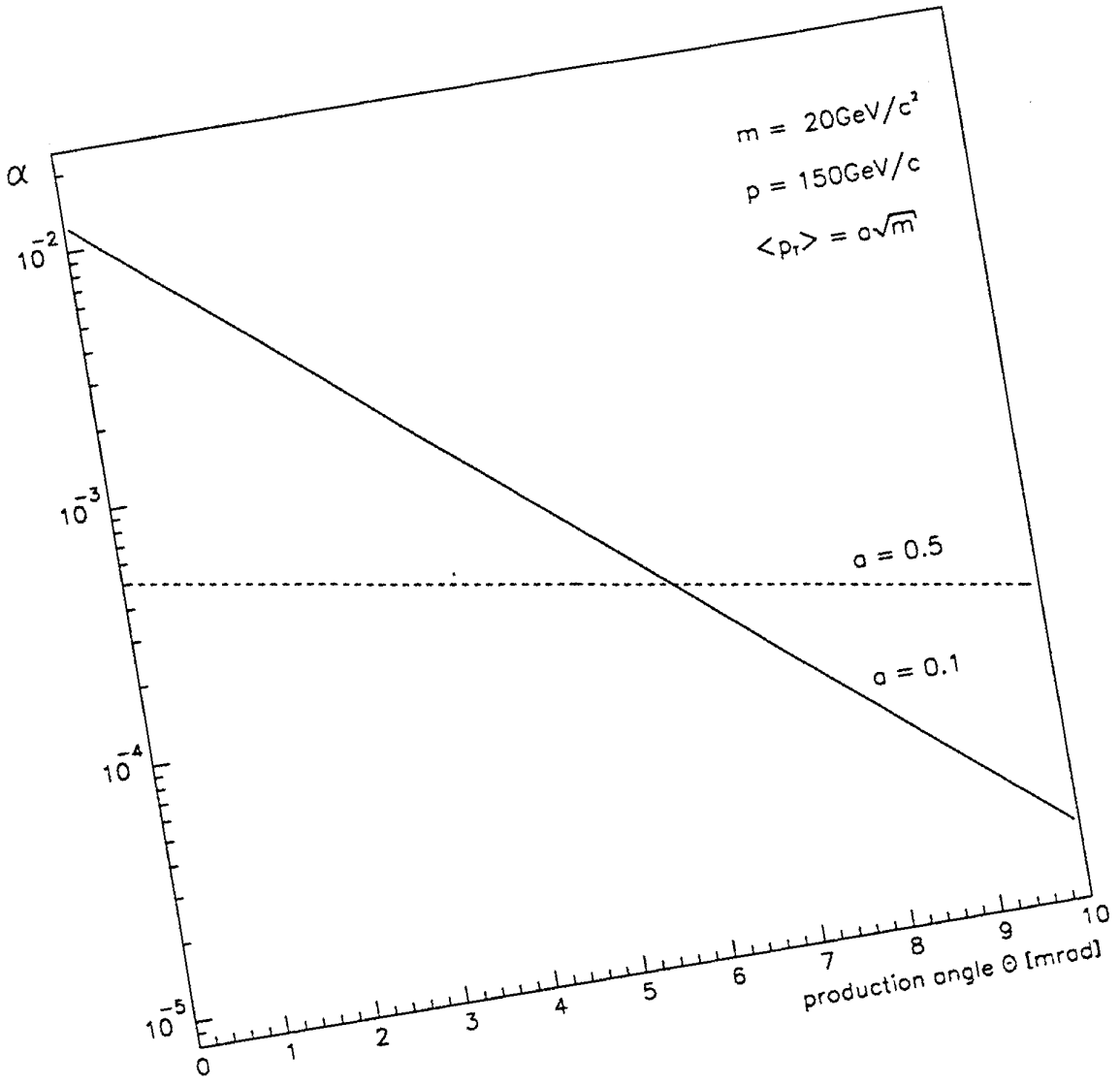

Fig.9 The acceptance α of the H_8-beam spectrometer versus the production angle for strangelets of mass 20 GeV/c^2, momentum 150 GeV/c and average transverse momentum, $\langle p_T \rangle = 0.5 \sqrt{m}$ and $\langle p_T \rangle = 0.1 \sqrt{m}$ GeV/c.

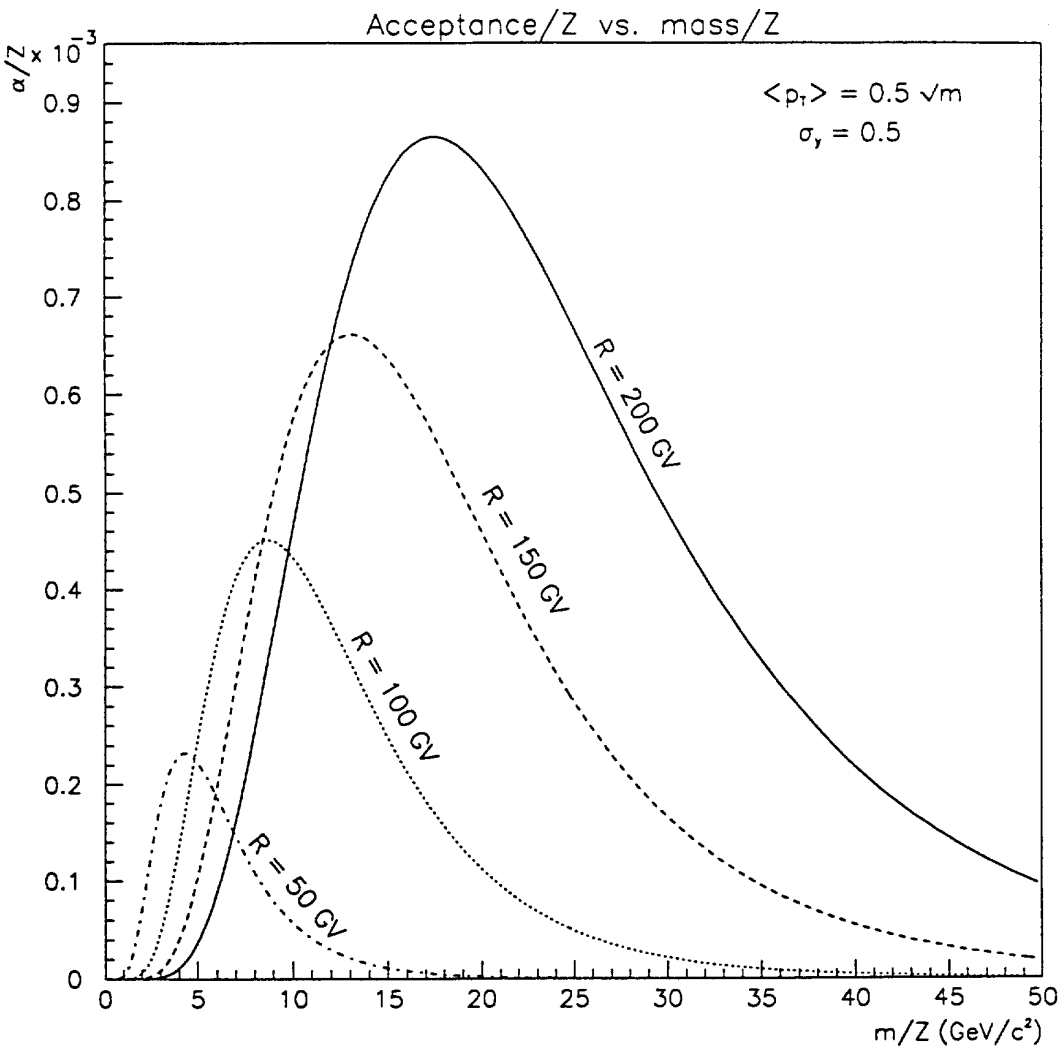

Fig.10 H_8-beam spectrometer acceptance α/Z versus m/Z for 0° production angle and rigidities R = 50, 100, 150, and 200 GV.

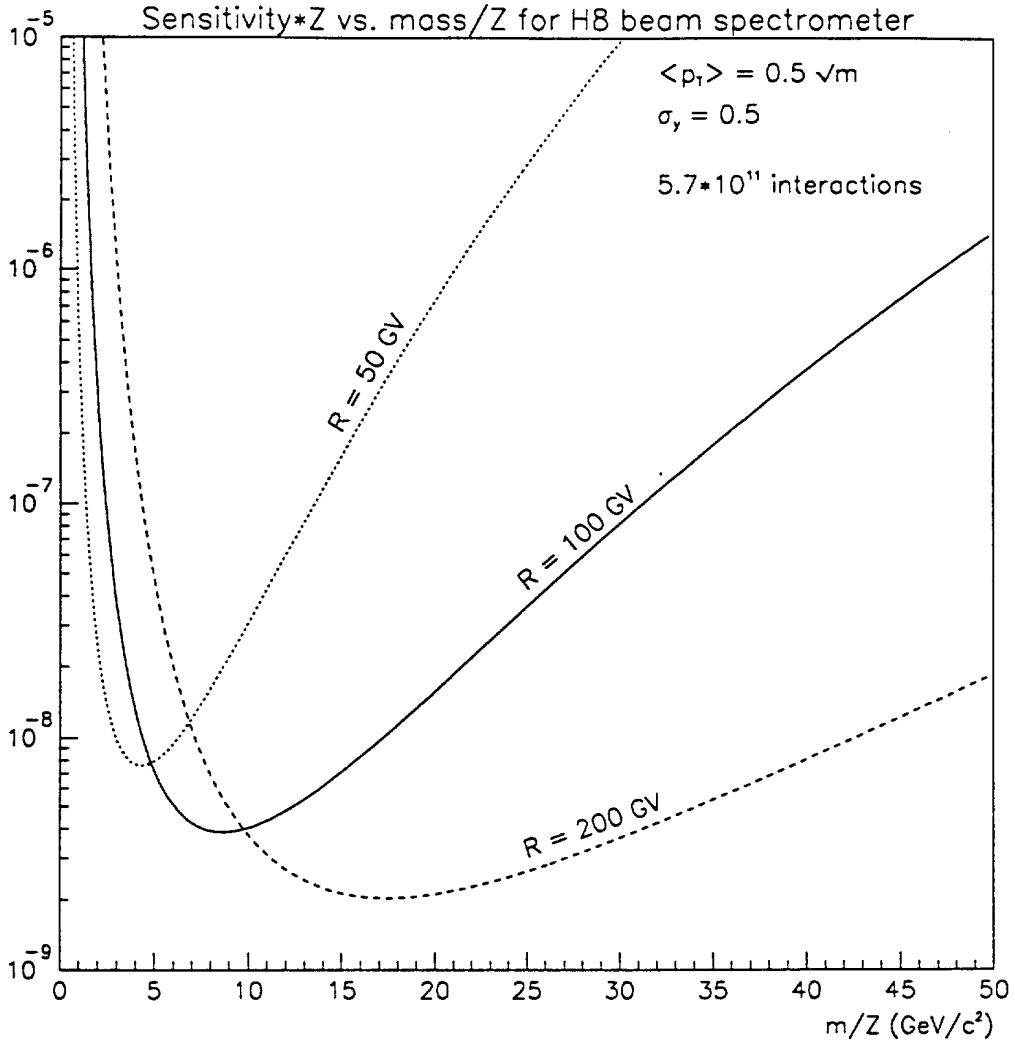

Fig.11 Detection sensitivity of strangelets at 0° production angle and $\langle p_T \rangle = 0.5 \sqrt{m}$ for spectrometer rigidities R = 200, 100, and 50 GV are shown as a function of m/Z. The detection efficiency is assumed to be $\varepsilon = 1$ in this plot. The sensitivities are calculated for $5.7 \cdot 10^{11}$ Pb-Pb interactions corresponding to 8 days of beam time.

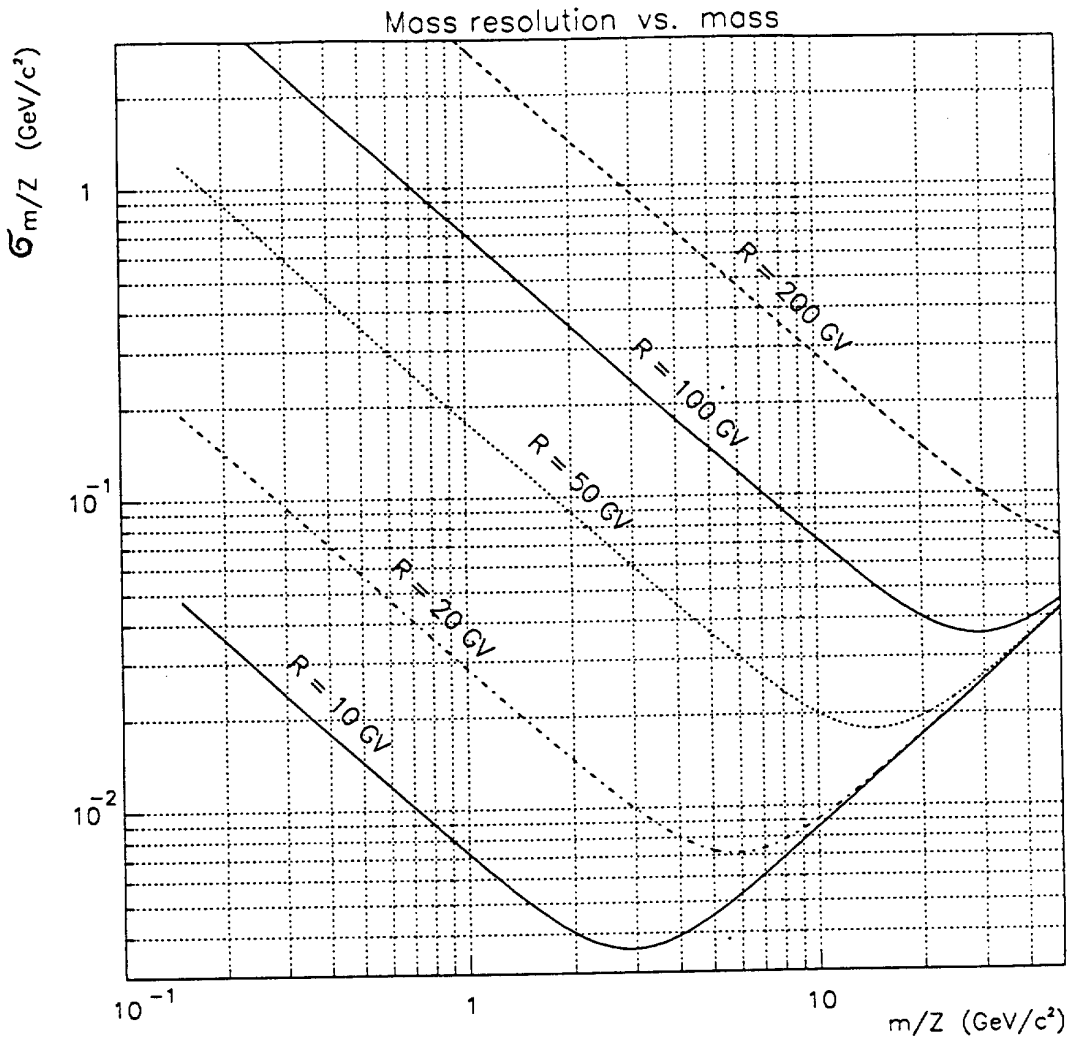

Fig.12 The mass resolution σ_m/Z as a function of m/Z for different spectrometer rigidities are shown.

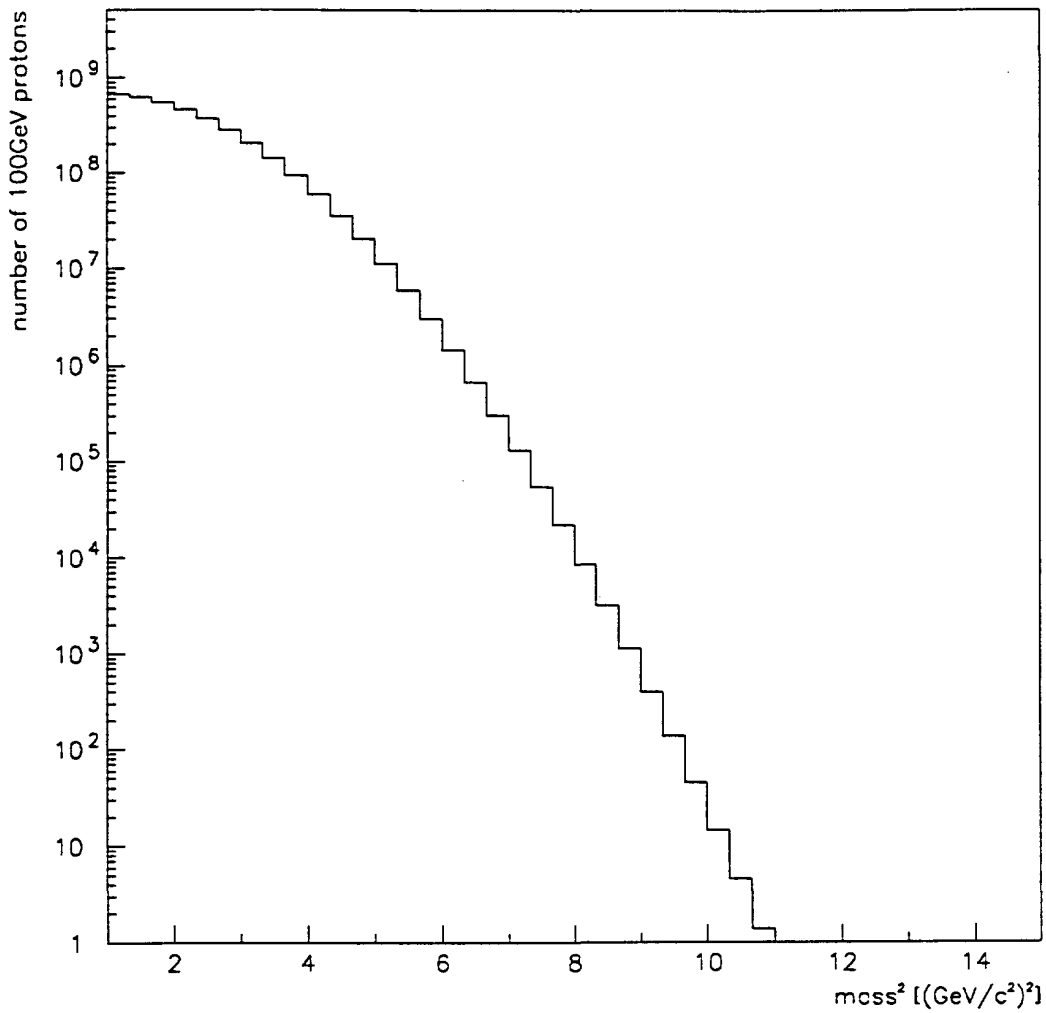

Fig.13 Mass distribution of protons with the rigidity R = 100 GV assuming purely Gaussian distributions of the TOF counter time resolutions. The number of protons are estimated from FRITIOF simulations and normalized to $5.7 \cdot 10^{11}$ Pb-Pb collisions.

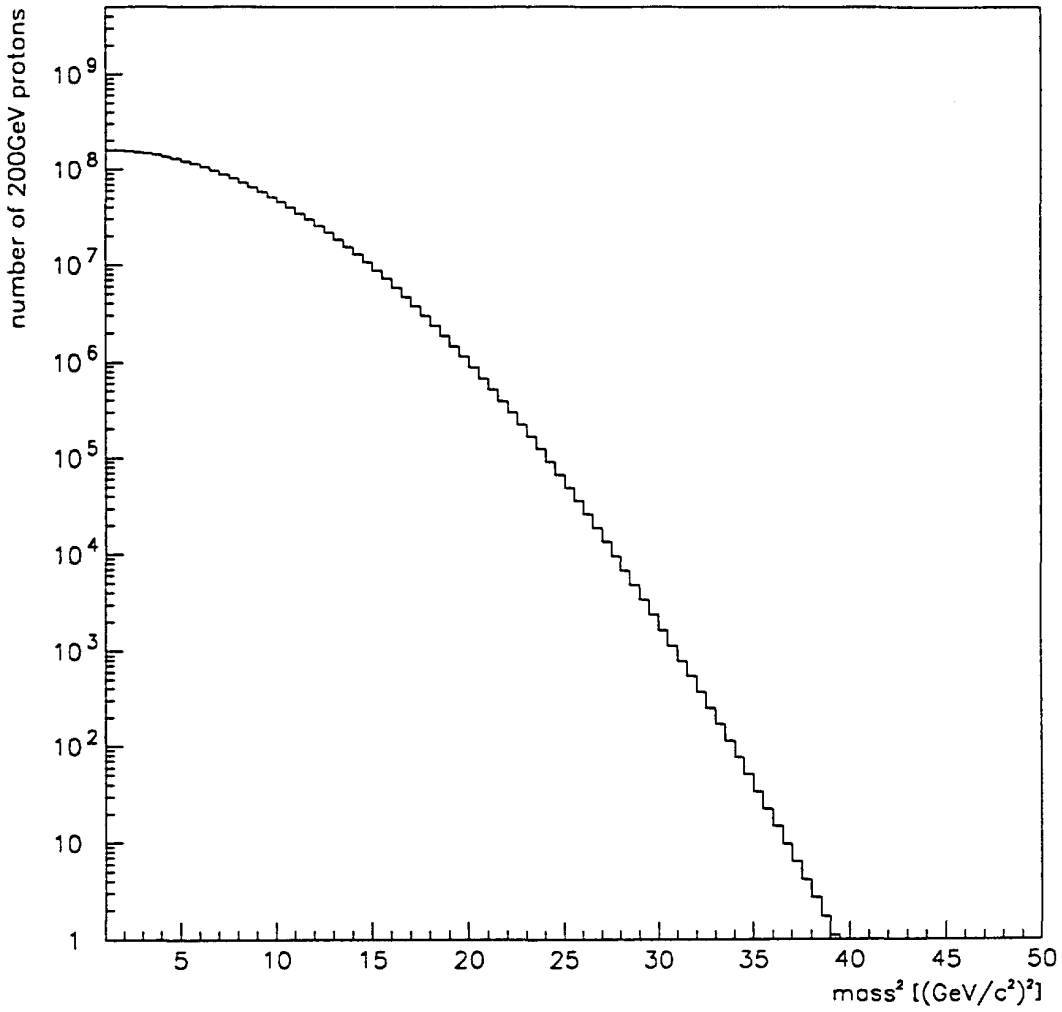

Fig.14 Mass distribution of protons with the rigidity R = 200 GV assuming purely Gaussian distributions of the TOF counter time resolutions. The number of protons are estimated from FRITIOF simulations and normalized to $5.7 \cdot 10^{11}$ Pb-Pb collisions.

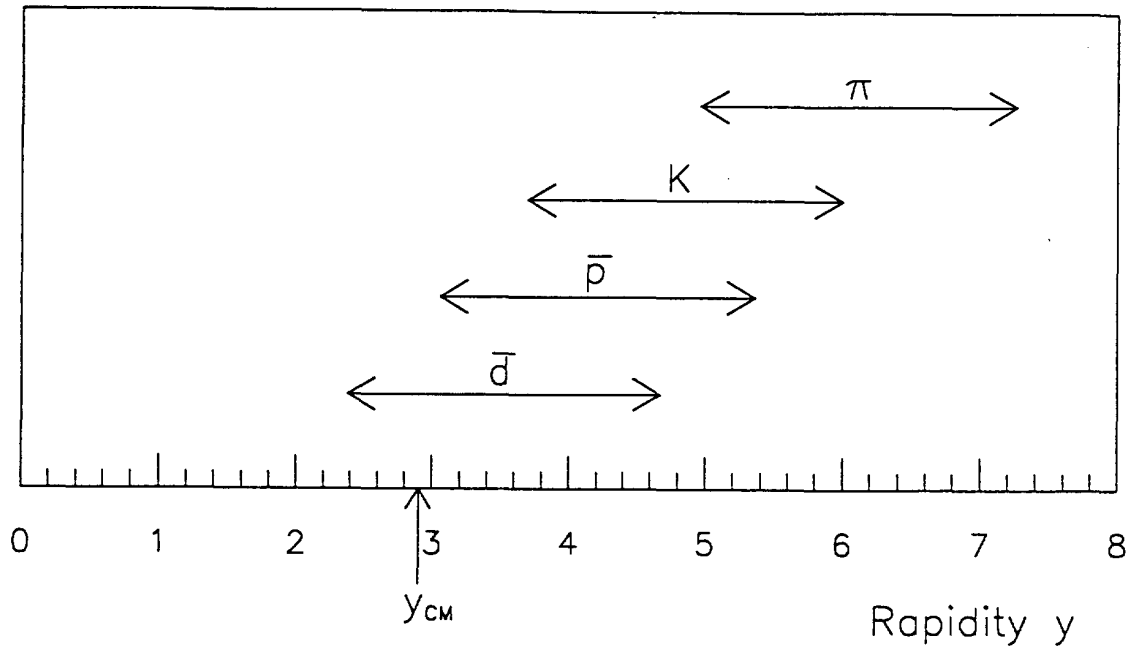

Fig.15 Rapidity range covered by the particle search.

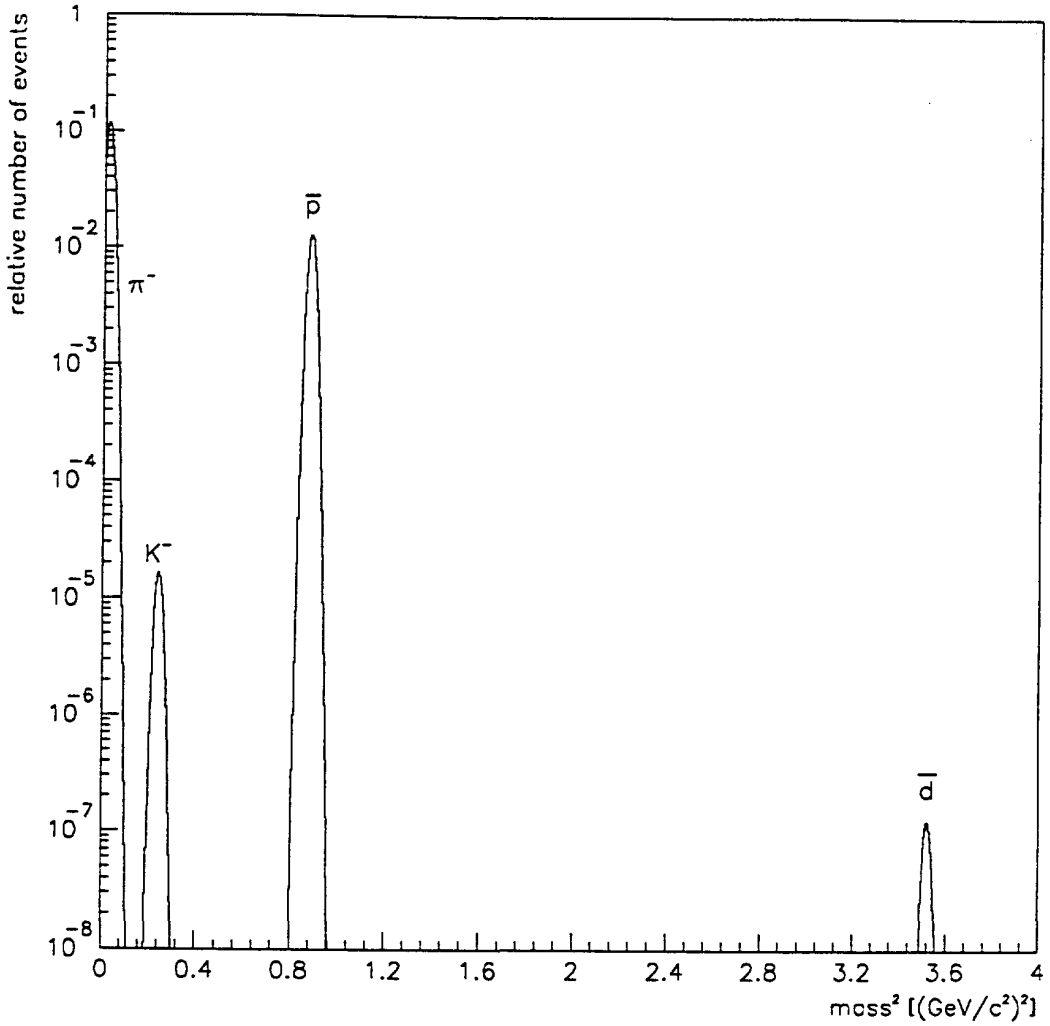

Fig.16 Time of flight measurement simulations using the relative particle yields from FRITIOF simulations at 10 GeV/c /Table 4). A $\bar{d}/\bar{p}$ ratio of 10^{-5} was assumed.

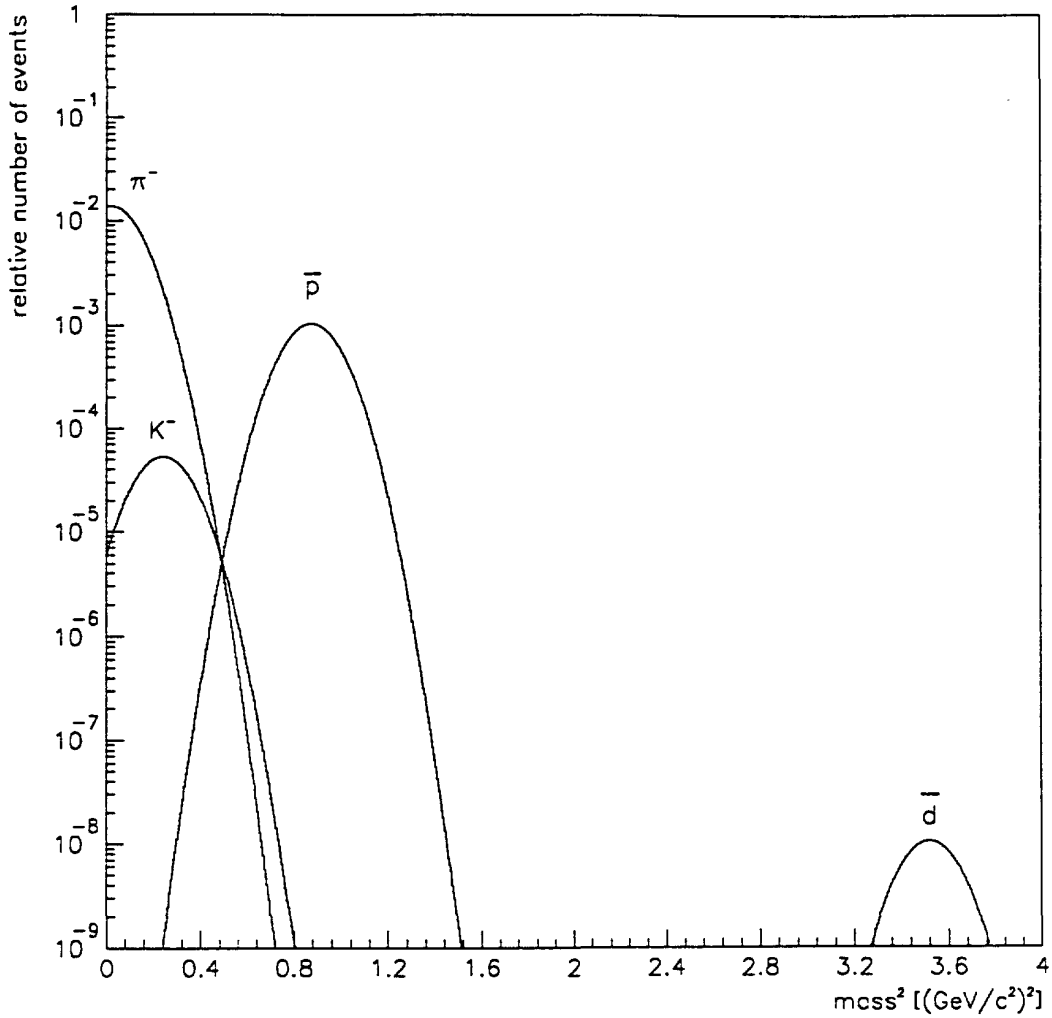

Fig.17 Time of flight measurement simulations using the relative particle yields from FRITIOF simulations at 28 GeV/c (Table 4). A $\bar{d}/\bar{p}$ ratio of 10^{-5} was assumed.